Efficient Synthesis of Organosulfur Compounds via Electrochemical Biomass Conversion

Qing Xia[1,2,3#], Xin Gao[1,2#], Jie Wu[1], Xinzhong Wang[1], Yanjie Zhai[1], Shanhe Gong[1], Weisong Li[1], Xiao Zhang[1,2,3*]

[1]*Department of Mechanical Engineering, The Hong Kong Polytechnic University, Hung Hom, Kowloon, Hong Kong SAR*

[2]*Research Institute for Advanced Manufacturing, The Hong Kong Polytechnic University, Hung Hom, Kowloon, Hong Kong SAR*

[3]*Research Institute for Smart Energy, The Hong Kong Polytechnic University, Hung Hom, Kowloon, Hong Kong SAR*

[*]Corresponding author: Xiao Zhang

E-mail: xiao1.zhang@polyu.edu.hk

Abstract

Artificial C-S bond formation plays a pivotal role in the preparation of drugs and their intermediates. Utilizing an electrochemical method powered by renewable energy offers a sustainable pathway to produce organosulfur compounds, but challenged by the low faradic efficiency (<6.8%) and production rate (< 10 μmol cm^{-2} hr^{-1}). In this study, we developed an efficient electrochemical approach to build C-S bonds and prepare a broad range of C-S species in high yield by coupling biomass oxidation with an S-containing nucleophile using commercial catalysts. Taking methanol as a representative, we successfully synthesized hydroxymethanesulfonate (HMS), sulfoacetate (SA), and methanesulfonate (MS). This system achieved a remarkable faradaic efficiency of over 95% within a low current density below 10 mA cm^{-2}. At commercial current densities ranging from 100-1000 mA cm^{-2}, the faradaic efficiency remained consistently over 60% in a practical flow reactor and high production rates, with stable operation over 50 hours without significant voltage increases or yield decreases at 100 mA cm^{-2}. Four reaction pathways, with *CH_2O, *CH_3, and *$OHCH_2CHO$ as key intermediates have been identified to facilitate the C-S bond formation. Impressively, this process can be effortlessly extended to synthesize a wide range of organosulfur and organonitrogen compounds from diverse feedstocks, achieving impressive production rates. Our approach promises to revolutionize the production of pharmaceuticals, textile chemicals, and agrochemicals.

Introduction

Organosulfurs are pervasive throughout natural ecosystems and various living organisms.[1] Over a thousand such compounds have been identified and extracted from terrestrial and aquatic sources, contributing significantly to the development of anticancer agents,[2,] anticonvulsants,[3] and antibacterial agents.[4] The market for organosulfur compounds is currently experiencing growth and is anticipated to continue its expansion at a notable Compound Annual Growth Rate (CAGR), encompassing both natural and synthetic varieties.[5] As an example, methanesulfonate has a market of 50 million USD and is projected to reach 72 million USD by 2032 with applications in electroplating, pharmaceuticals, and esterification.[6] These compounds continue to be influential in the discovery of novel pharmaceuticals, underscoring their vital role in advancing medical science and other areas.[7,8]

In light of their importance,[9-12] continuous efforts are being made in the artificial synthesis of organosulfur compounds, with the sulfa-Michael addition reaction,[13 14] Diels-Alder reaction[15,16] and allylic sulfonation,[17,18] being examples of effective approaches. While these methods are able to create carbon-sulfur (C–S) bonds, they often require metal-ligand complexes or highly pre-functionalized precursors and are typically energy-intensive, relying on substantial fossil energy usage.[1] Moreover, they utilize extracted substances like alkenes and ketenes as reactants, generating a significant amount of CO_2 during the production process (**Fig. 1a**).[19,20] Therefore, a critical task in the formation of C-S bonds is to streamline the reaction process in an environment-friendly way and reduce both energy consumption and overall costs. The electrochemical formation of C-S bonds using renewable energy sources offers a promising solution to this challenge.[21,22] It was reported that electrochemically coupling S-containing nucleophiles with activated electrophilic intermediate (CHOH) from CO_2 reduction on a Cu-based catalyst is available for generating the C-S bonds (**Fig. 1b**).[21] However, the approach is constrained by a low faradaic efficiency (FE) of less than 6.8% and a consistently low production rate across various currents. Additionally, the lack of commercially viable catalysts and the limitation in extending the method to other carbon-based products further complicate the scalability of manufacturing C-S

compounds on an industrial level.

Herein, we developed an efficient electrochemical approach for constructing C-S bonds and synthesizing C-S compounds with extremely high yields by using commercially available catalysts. This was achieved by driving the oxidation reaction of biomass-derived feedstocks in an S-containing nucleophile electrolyte. By utilizing the CH_3OH and SO_3^{2-} as feedstock with the Ketjen Black (KB) as the catalyst, our method achieved over 95% FE for C-S species at a current density of below 10 mA cm^{-2}, and maintained over 80% FE at 75 mA cm^{-2}. During the reaction, the electrophilic intermediates $*CH_2O$, $*CH_3$, and $*OHCH_2CHO$will be generated and rapidly react with SO_3^{2-}, thus promoting the formation of various C-S compounds. Furthermore, the system is able to continuously produce C-S species in an industry-available scale with a high production rate of 6959.76 μmol cm^{-2} hr^{-1} for production at 1 A cm^{-2}, and maintain a nearly 80% FE at an industrial current density of 100 mA. Importantly, this approach can be adapted to construct a diverse array of C-S and C-N species from various feedstocks (such as ethanol, acetate, isopropanol, glycolic acid, glycerol, and ethylene glycol) at considerably high production rates. Our findings hold the potential to significantly impact the production of these essential compounds, offering wide-ranging benefits to the fields of pharmaceuticals, energy, and environmental science.

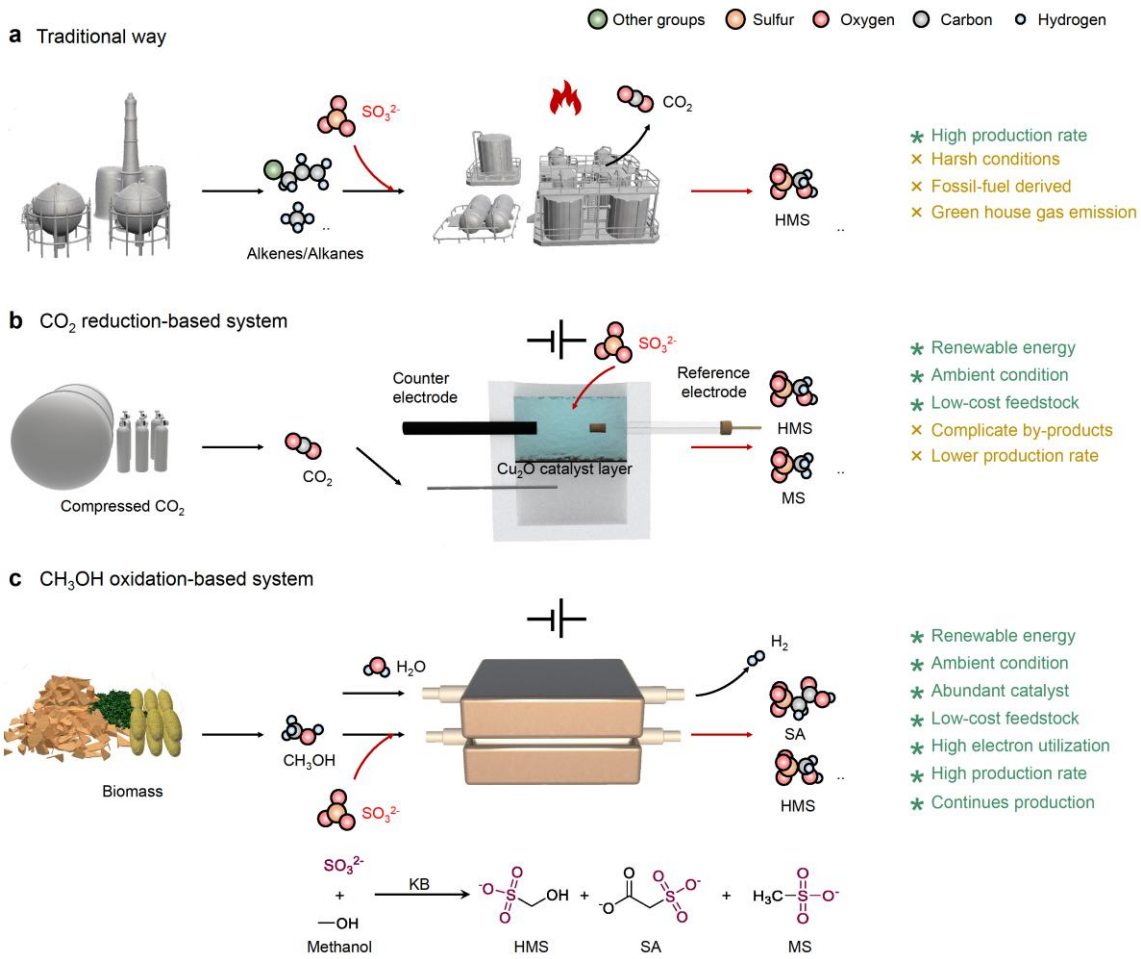

Fig. 1 | **(a)** Schematic representation of the traditional method, **(b)** electrochemical CO_2-reduction based approach, and **(c)** our approach (CH_3OH oxidation as an example) for C-S bond construction.

Result and discussion

Reaction design and catalyst selection:

Electrochemical construction of C-R bonds is a promising approach for synthesizing carbon-based chemicals, typically necessitating two feedstocks: An R-containing nucleophile and a carbon-based activated electrophilic intermediate. Our approach for C-S bond formation leverages the in-situ generation of this electrophilic intermediate through the biomass oxidation process, facilitating its reaction with an S-containing nucleophile within the electrolyte. To demonstrate the process simply, we first choose the abundant CH_3OH as a representative reactant, which can be sourced not only from fossil fuels through the Fischer-Tropsch process but also from biomass

via thermocatalytic and biocatalytic methods.[23-25] Additionally, it offers advantages such as low economic value, a straightforward oxidation pathway, and lower oxidation potential.[26] As shown in **Fig. 1c**, the C-S coupling reaction occurred at the anode, and a hydrogen evolution reaction (HER) took place as the cathodic reaction. During electrolytic reaction, the CH_3OH was oxidized and generated activated electrophilic intermediates such as $*CH_2O$, and $*CH_3$ at the catalyst surface. These intermediates can rapidly react with SO_3^{2-}, resulting in the formation of C-S species. To drive the reaction efficiently and economically, commercially available catalysts are preferred. In our design, the commercial carbon, KB, was selected to drive the anodic C-S coupling reaction, and the commercial Pt was used as the cathode catalyst.

Performance evaluation and optimization for C-S species production

To prove the above concept, we first utilized a three-electrode cell to validate the C-S bond formation by conducting CH_3OH oxidation in an S-containing nucleophile (here is SO_3^{2-}) electrolyte. The KB catalysts with particle sizes of around 50 nm are uniformly coated on the TGP-60 carbon paper as the electrode (**refer to Fig. 2a and Supplementary Fig. 1 for additional details**). The linear sweep voltammetry (LSV) was conducted to evaluate the potential activity of the C-S bond formation reaction. **As illustrated in Fig. 2b and Supplementary Fig. 2** in an electrolyte containing both Na_2SO_3 and CH_3OH, a distinct electrocatalytic behavior at the anode was observed, in contrast to electrolytes containing only one of the mentioned species. Specifically, an onset potential of 0.9 V versus RHE was recorded in the electrolyte containing 0.2 M Na_2SO_3 + 1.0 M CH_3OH, which falls between the onset potential observed with 0.2 M Na_2SO_3 alone (1.2 V vs. RHE) and with a mixture of NaOH and 1.0 M CH_3OH (0.53 V vs. RHE. PH = 10, match the 0.2 M Na_2SO_3 + 1.0 M CH_3OH electrolyte). The low potential in NaOH + 1.0 M CH_3OH indicates the occurrence of the CH_3OH oxidation reaction, while the high potential in the 0.2 M Na_2SO_3 electrolyte corresponds to the SO_3^{2-} oxidation reaction (SOR). The slightly higher onset potential observed in the 0.2 M Na_2SO_3 + 1.0 M CH_3OH mixture can be attributed to the blocking effect of SO_3^{2-}, which suppresses CH_3OH oxidation. This suppression is also observed, and even more

evident, in electrolytes containing other anions such as SO_4^{2-}, CH_3COO^-, and HCO_3^-, (**Supplementary Fig. 3a-c**). Beyond 0.9 V, we speculate that not only does CH_3OH oxidation occur, but also C-S bond formation is initiated through the reaction between CH_3OH oxidation intermediates and SO_3^{2-}. In this process, the adsorbed CH_3OH on the catalyst surface is converted to an electrophilic intermediate, which then reacts with SO_3^{2-}. By increasing the CH_3OH concentration to 8.0 M, the current density increased in the low potential range from 0.9 to 1.4 V *vs.* RHE, which indicates more intermediates are generated resulting from the high concentration of CH_3OH. While at the high potential range of above 1.4 V, the high concentration of the CH_3OH suppressed the SOR and thus a lower current density was exhibited compared with that in 0.2 M Na_2SO_3 + 1.0 M CH_3OH anolyte.

Although the aforementioned findings show the feasibility of C-S bond formation, direct evidence of this process remains absent. Therefore, we further employed the 2D ^1H-^{13}C HSQC spectroscopy to directly ascertain the composition of the products. As shown in **Fig. 2c and Supplementary Figs. 4-7**, four different chemicals, namely hydroxymethane sulfonate (HMS, 4.44 ppm, 73.25 ppm), sulfoacetate (SA, 3.74 ppm, 57.22 ppm), methanesulfonate (MS, 2.82 ppm, 39.22 ppm), and formate ($HCOO^-$, 8.43 ppm, 172.27 ppm), were detected in the solid products after evaporation of the reacted electrolyte. Note that HMS, SA, and MS are all high-valuable C-S species that have been widely used in the textile industry, atmospheric chemistry, pharmaceuticals, and as additives.[21,27-29] To further verify the carbon sources of these products and determine the number of electrons transferred, isotope labeling experiments were conducted. As shown in **Supplementary Fig. 8a-b**, the ^1H NMR spectra exhibited clear shifts and splitting patterns in the carbon peaks corresponding to formate, HMS, SA, and MS when using ^{13}C-labeled methanol combined with ^{12}C catalysts. These shifts were absent when ^{12}C-methanol and ^{13}C-labeled catalysts were used, providing conclusive evidence that the carbon atoms in all key products originate from methanol. Based on these results, we can know that the formation of HMS, SA, MS, and $HCOO^-$ involves $2e^-$, $6e^-$, $2e^-$, and $2e^-$ transfer processes, respectively. These products were further quantified by ^1H-nuclear magnetic resonance (^1H-NMR, **Supplementary Fig. 9**), and other by-

products such as CO, CO_2, and the SO_4^{2-} were also detected and quantified by gas chromatography (GC), CO_2 meter and liquid chromatography-mass spectrometry (LC-MS) (**Supplementary Figs. 10-12**). Over the range of measured current densities from 5 to 200 mA cm^{-2}, over 70% of the electrons were utilized to oxidize SO_3^{2-} to SO_4^{2-}, with the faradaic efficiency for C-S species ($FE_{C\text{-}S\ species}$) initially increasing and then declining as the current density increased ((**Supplementary Fig. 13**)). Particularly at 75 mA cm^{-2}, the $FE_{C\text{-}S\ species}$ peaked at 20.72%, with HMS contributing 8.78%, SA 11.84% and MS accounting 0.10%, respectively. We observed that the FE_{MS} remained consistently low, typically below 1%, across all current densities. Additionally, HMS accounted for the majority of the C-S species, reaching 68.4%, while SA and MS contributed 30.8% and 0.8%, respectively. The majority of HMS indicate that this approach has promising applications in the fields of bioculture and atmospheric monitoring.[30,31] Considering the product rates of most C-S species, they modestly increased with higher current densities (**Supplementary Fig. 14**). At an industrial-available current density of 200 mA cm^{-2}, the production rate of C-S species can reach a high value of 420.4 μmol cm^{-2} hr^{-1}, much higher than that of traditional electrochemical CO_2 reduction approach with a rate of below 10 μmol cm^{-2} hr^{-1}.

To further enhance the production rate of C-S species, optimization experiments were conducted by first adjusting the CH_3OH concentration from 1.0 M to 8.0 M. The FE for HMS, SA, and MS obtained from different electrolytes were collected and analyzed at 5-200 mA cm^{-2} (**Figs. 2d-f**). For HMS production, it is clear that the FE_{HMS} increases firstly and then decreases with increasing concentration of CH_3OH. The optimized FE_{HMS} reaches 15.30% in electrolyte with 4.0 M CH_3OH at 75 mA cm^{-2}. At a low current density of 5 mA cm^{-2}, SA became the dominant product when the CH_3OH concentration reached 8.0 M, with FE_{SA} peaking at over 92%, while the combined FE for HMS and MS remained below 3%. The high selectivity for a single product indicates the potential to deplete the reactants gradually, resulting in a product of higher purity over an extended reaction period. For MS generation, the FE_{MS} positively correlates with methanol concentration, but the overall efficiency remains notably low, under 2.0% across all current densities (**Fig. 2f**), and the maximum molar proportion of

MS, approximately 5.4%, is attainable at 75 mA cm^{-2} in an electrolyte containing 8.0 M CH_3OH (**Fig. 2g**). The overall FE for C-S bond formation suggests that high methanol concentrations significantly promote C-S bond formation, while the main side reaction of the SOR was drastically suppressed, decreasing from nearly 80% to below 10% (**Supplementary Fig. 15 and Fig. 2g**). Specifically, in an electrolyte containing 8.0 M CH_3OH (**Fig. 2g**), the overall FE for C-S species was over 75% at lower current densities ranging from 5-75 mA cm^{-2}, peaking at 95.10% at 5 mA cm^{-2}. Impressively, high FE values above 65% were also achieved at current densities between 100-200 mA cm^{-2}. Additionally, unprecedented production rates were observed at 200 mA cm^{-2}: 1177.72 μmol cm^{-2} hr^{-1} for C-S species overall, with 406.78 μmol cm^{-2} hr^{-1} for HMS and 716.78 μmol cm^{-2} hr^{-1} for SA **(Fig. 2g and Supplementary Fig. 16)**. We also observed that adding 0.5 M $NaHCO_3$ to the electrolyte as a pH buffer did not significantly affect the overall product distribution across various current densities and methanol concentrations (**Supplementary Fig. 17**).

The formation of C-S bonds depends on the reaction of generated electrophilic intermediates with S-containing nucleophiles. Therefore, the concentration of SO_3^{2-} also plays a crucial role in affecting the production rate of HMS, SA, and MS. To maximize the overall electron utilization and production rate, the SO_3^{2-} concentration was further optimized. As shown in **Fig. 2h**, at 100 mA cm^{-2}, an increase in SO_3^{2-} concentration leads to a reduction in HMS formation while enhancing SA production, without affecting MS production. Specifically, as SO_3^{2-} concentration increased from 0.1 to 0.5 M, the FE for HMS dropped from 30.70% to 0.32%, and the FE for SA rose from 40.67% to 61.12%. For all C-S species combined, the FE and production rate peaked at 72.04% and 838.14 μmol cm^{-2} hr^{-1}, respectively, in a solution of 0.1 M Na_2SO_3 + 8.0 M CH_3OH at 100 mA cm^{-2}, aligning with efficient production standards suitable for industrial-scale currents.

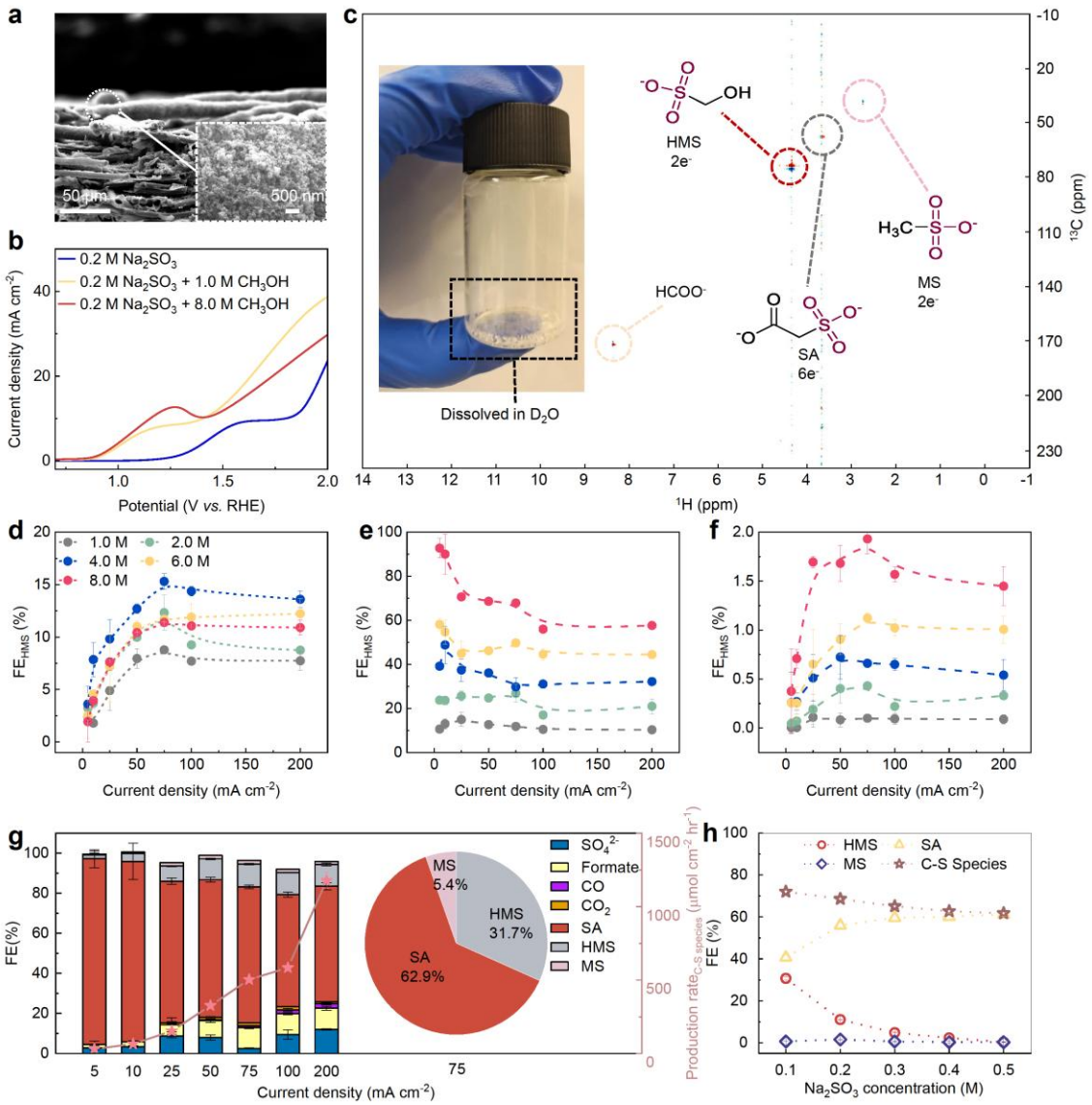

Fig. 2 | Electrochemical performance of KB for C-S construction. (a) SEM images of the KB-coated carbon paper, the inset image shows the morphology of KB. **(b)** Linear sweep voltammetry (LSV) curves of KB in different electrolytes. **(c)** The 2D ^{1}H-^{13}C HSQC spectrum of the products obtained from the reacted electrolyte. The ^{1}H and ^{13}C patterns are shown on the horizontal axis and the vertical axis, respectively. The FEs of **(d)** HMS, **(e)** SA, and **(f)** MS in electrolytes with different concentrations of CH_3OH. **(g)** FEs of different products were obtained at 5-200 mA cm^{-2} in 0.2 M Na_2SO_3 + 8.0 M CH_3OH, and the inset pie chart shows the molar ratios of different C-S products at 75 mA cm^{-2}. **(h)** FEs of HMS, SA, MS and C-S species for the electrolyte with different concentrations of Na_2SO_3 at 100 mA cm^{-2}. All the tests were conducted without IR compensation. The error bars represent at least three independent tests.

Pathway for C-S bond construction

The high yield and production of C-S compounds motivate us to further explore the possible mechanism of C-S formation in our design, and the elucidation of key intermediates and reaction pathways is also crucial for enhancing production rates and promoting this method to prepare other C-related species. To this end, we integrated in-situ experimental analysis with density functional theory (DFT) calculations to decipher the mechanisms of C-S bond formation.[32,33] We first employed in-situ attenuated total reflectance surface-enhanced infrared absorption spectroscopy (ATR-SEIRAS) to monitor changes in intermediates and ions at the interface during the reaction in a solution of 0.1 M Na_2SO_3 and 2.0 M CH_3OH, as shown in **Fig. 3a**. Additionally, to better distinguish the peaks, control experiments were performed by acquiring spectra in the absence of sulfite or methanol (**Supplementary Fig. 18a-c**). We observed multiple peaks that increased in intensity with higher potentials, indicating various chemical interactions. Peaks at 1520 and 1509 cm^{-1} are associated with surface-bound SO_3^{2-} species, while peaks at 1699 and1540 cm^{-1} are indicative of surface sulfate species.[34-39] These species indicate that a significant quantity of SO_3^{2-} ions will be adsorbed onto the catalyst surface under positive potential, serving as a sulfur source for the formation of C-S bonds. Peaks at 1635 and 1684 cm^{-1} were linked to HCO_3^- adsorption.[40] Additionally, a peak at 1454 cm^{-1} was identified as CO_3^{2-},[41] while peaks within the 1800-2000 cm^{-1} range were attributed to *CO.[42,43] These species suggest that over-oxidation of CH_3OH to CO_2, which then reacts with OH^- to form HCO_3^- and CO_3^- ions, contributes to the decreased yield of C-S products under high-current conditions. Additionally, certain prominent peaks were indicative of the formation of intermediates and products involved in the reaction process. The presence of peaks at 1320, 1716, and 1770 cm^{-1} signaled the involvement of the *COOH intermediate peaks, indicating the formation of the formate and SA.[44-46] A distinct peak at 1474 cm^{-1} suggests the presence of $*CH_2O$, as previously reported.[47] Additionally, a strong signal at 1750 cm^{-1} is associated with *CHO species,[48] resulting from the further oxidation of $*CH_2O$. which arise from the further oxidation of $*CH_2O$. These activated electrophilic intermediates likely contribute to C–S bond formation. To elucidate the potential

pathways for C-S bond generation, we combined theoretical conjectures with experimental validation.

The transformation of CH_3OH to HMS involves a loss of 2 electrons, which also occurs during $*CH_2O$ formation, thus we speculate that $*CH_2O$ may serve as a key intermediate in HMS formation. To validate this hypothesis, we directly introduced formaldehyde (CH_2O) into various solutions (**Supplementary Fig. 19**). The resulting ^1H NMR spectra demonstrated that CH_2O spontaneously reacts with SO_3^{2-} to form HMS, without SA detected. This suggests the involvement of intermediates other than CH_2O in SA formation. Based on the above discussion, we propose mechanisms for HMS formation as elucidated by DFT calculations. As depicted in **Fig. 3b**, the process undergoes a sequence like $*CH_3OH \rightarrow *CH_3O \rightarrow *CH_2O \rightarrow *HOCH_2SO_3^-$ (**Equations 1-5**), with most steps occurring spontaneously, except for $*CH_3O$ formation and HMS desorption. Additionally, considering the kinetics, the $*CH_2O \rightarrow *HOCH_2SO_3^-$ step exhibits a significantly lower energy barrier compared to the successive $*CH_2O$ oxidation step, further supporting the results (**Supplementary Fig. 20**). Beyond the reaction between $*CH_2O$ and $*SO_3^{2-}$, we also investigated whether SA could undergo further oxidation, leading to C-C-S bond cleavage and the formation of HMS. However, the ^1H NMR results shown in **Supplementary Fig. 21** demonstrate that SA is highly stable and does not serve as a precursor for HMS formation

$$CH_3OH + * \rightarrow *CH_3OH \quad (1)$$

$$*CH_3OH \rightarrow *CH_3O + H^+ + e^- \quad (2)$$

$$*CH_3O \rightarrow *CH_2O + H^+ + e^- \quad (3)$$

$$*CH_2O + SO_3^{2-} \rightarrow *CH_2O/SO_3^{2-} \quad (4)$$

$$*CH_2O/SO_3^{2-} + H^+ \rightarrow *HOCH_2SO_3^- \quad (5)$$

For SA formation, understanding the sequence of bond formation, specifically, whether the C-S or C-C bond forms first, is pivotal for elucidating the synthesis of multicarbon sulfides. To investigate the hypothesis that C-C bond formation precedes C-S bond creation, we utilized an electrolyte solution of 0.2 M Na_2SO_3 and 8.0 M CH_3OH. Following 20 hours of electrolysis at 5 mA cm^{-2}, the predominant C-S species formed was SA, with negligible amounts of HMS and MS (**Supplementary Fig. 22**).

This suggests that C-C-S compounds can be synthesized even in the absence of significant C-S products, supporting the hypothesis of initial C-C bond formation. To investigate potential C_2 intermediates formed during the reaction, we employed differential electrochemical mass spectrometry (DEMS). As shown in **Supplementary Fig. 23**, a significant signal corresponding to the intermediate $*HOCH_2CHO$ (m/z = 60) was detected, indicating its formation through the coupling reaction of $*CH_2OH$ and *CHO. Based on these findings, we propose a reaction pathway, depicted as the blue path in Fig. 3b (Path 3). In this pathway, $*CH_2OH$ and *CHO are first generated and subsequently combine to form a C–C bond (**Equations 6–8**), which undergoes five additional steps to produce SA (**Equations 9–12 and Equation 1**).

$$*CH_2O \rightarrow *CHO + H^+ + e^- \quad (6)$$

$$*CH_3OH \rightarrow *CH_2OH + H^+ + e^- \quad (7)$$

$$*CH_2OH + *CHO \rightarrow *HOCH_2CHO \quad (8)$$

$$*HOCH_2CHO + SO_3^{2-} \rightarrow *HOCH_2CHO/SO_3^{2-} \quad (9)$$

$$*HOCH_2CHO/SO_3^{2-} + H^+ \rightarrow *HOCH_2CHOHSO_3^- \quad (10)$$

$$*HOCH_2CHOHSO_3^- \rightarrow *HOCCH_2SO_3^- + H_2O \quad (11)$$

$$*HOCCH_2SO_3^- + H_2O \rightarrow *HOOCCH_2SO_3^- + 2H^+ + 2e^- \quad (12)$$

Conversely, considering the possibility of C-S bond formation occurring first, we propose that HMS may undergo further oxidation and then couple with other intermediates to form a C-C-S bond. ^1H NMR spectra show that HMS is not stable under high current density, as the C-S bond in HMS cleaves, producing small amounts of formate as the product (**Supplementary Fig. 24**). Moreover, when an electrolyte containing 0.2 M HMS and 8.0 M CH_3OH was used, and electrolysis was conducted for 20 hours at a current density of 5 mA cm^{-2}, methyl formate and formate were produced, with no detection of SA (**Supplementary Fig. 25**). This outcome aligns with the oxidation process of 8.0 M CH_3OH alone (**Supplementary Fig. 26**), indicating that HMS may only function as a conductive ion, further suggesting that this proposed pathway is incorrect.

The formation of MS presents an intriguing case when examining the valence states of the reactants (CH_3OH, SO_3^{2-}) and the product ($CH_3SO_3^-$), where the valence

of the carbon does not change. This observation raises the possibility that the reaction could be either a standard chemical reaction or a thermochemical reaction triggered by the heat from the electrical current passing through the catalyst. To evaluate our hypothesis, we introduced 2 M CH_3OH into a 0.2 M Na_2SO_3 solution containing KB and subjected the mixture to varying temperatures ranging from 20-80 ℃ for 10 hours. We then employed ^1H NMR spectroscopy to identify potential products in the different solutions. As shown in **Supplementary Fig. 27**, there is no MS detected in all the above solutions, indicating that MS formation likely necessitates electron involvement, thus characterizing it as an electrochemical process. It is also crucial to note that the production of MS is exceedingly limited, contributing to only about 1% of the total molar proportion of all C-S products. So we believe that during the formation of $CH_3SO_3^-$, CH_3O is first produced through the oxidative dehydrogenation of CH_3OH. Subsequently, CH_3 and O are generated through homolytic cleavage of the radical. Then, $*SO_3^-$, produced by single-electron oxidation, reacts with $*CH_3$ via a radical addition reaction to form $CH_3SO_3^-$. Although the oxidation states of the elements in the reactants and products remain consistent, multiple high-energy steps are required to form the final product (**Supplementary Fig. 28**). We theorize that this reaction could result from the interaction of active $*CH_3$ intermediates with $*SO_3^{2-}$ (**Equations 13-15**). However, the formation of the $*CH_3$ intermediate appears to be highly challenging, leading to diminished MS yields.

$$*CH_3O \rightarrow *CH_3 + *O \quad (13)$$

$$* + SO_3^{2-} \rightarrow *SO_3^- + e^- \quad (14)$$

$$*CH_3 + *SO_3^- \rightarrow *CH_3SO_3^- \quad (15)$$

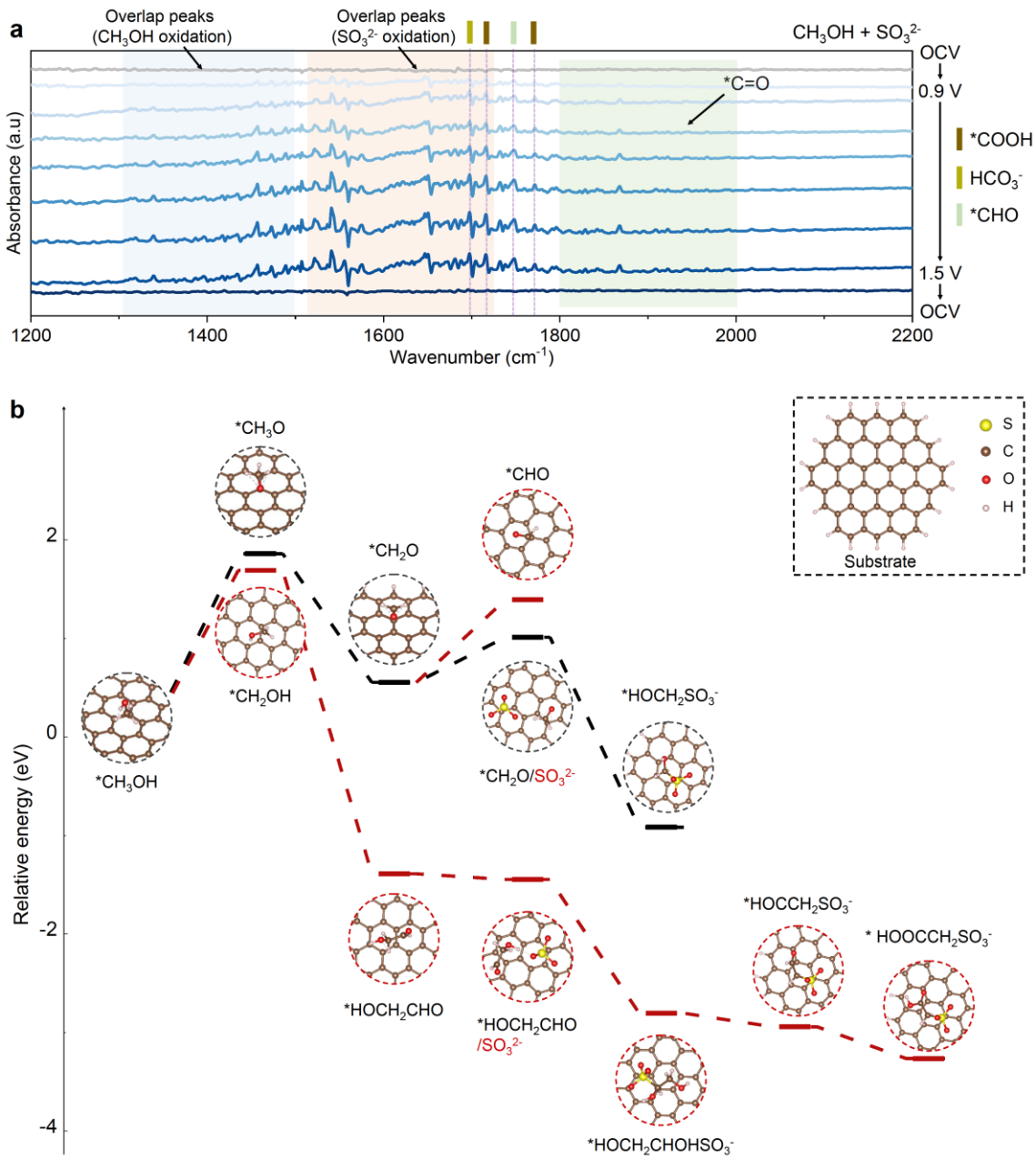

Fig. 3 | Mechanism investigation for C-S bond construction on KB catalysts. (a) ATR-SEIRAS spectra during C-S bond formation in 0.1 M Na_2SO_3 + 2.0 M CH_3OH electrolyte. **(b)** The Gibbs free energy diagrams for possible routes to C-S bond formation.

Continues electrosynthesis C-S species in a practical flow reactor

To continue the production of C-S species in a practical way, a membrane electrode assembly (MEA) reactor was assembled by coupling HER and C-S bond formation reaction. As shown in **Fig. 4a**, the reactor comprises a cathode (KB) and an anode (Pt/C),

separated by a Nafion-117 proton exchange membrane. The DI water was continuously supplied in the cathode side for HER, while the anode side was fed with a 0.1 M Na_2SO_3 + 8.0 M CH_3OH solution. The I-V curve, covering a current density range of 10-1000 mA cm^{-2}, is depicted in **Fig. 4b**. The steep increase in current density with rising cell voltage suggests that mass limitations were minimized in this flow reactor, even at industrial current densities. In addition, at 100 mA cm^{-2}, the overall cell voltage was only 3.08 V, achieving an FE for C-S species of over 80% and a high production rate of 871.67 μmol cm^{-2} hr^{-1} (**Fig. 4c**). When the current densities exceeding 300 mA cm^{-2}, the FE for C-S species slightly decreases to 70%, driven by the increasing prevalence of the SOR side reaction, along with the enhanced production of formate and gases (CO and CO_2). Nevertheless, the production rate of C-S species remains at a high value of over 1921.19 μmol cm^{-2} hr^{-1}, sufficient for industrial needs. Impressively, a production rate of 6959.76 μmol cm^{-2} hr^{-1} was achieved at a current density of 1000 mA cm^{-2} (**Fig. 4d**), which is approximately 818.79 times higher than those reported for CO_2-based systems (**Supplementary Fig. 29**). Moreover, this reactor can be steadily operated for over 50 hours for continuously producing C-S species, maintaining an FE of nearly 80% at 100 mA cm^{-2} without obvious decay (**Fig. 4e**), which is promising for industrial-scale production requirements.

The unprecedented performance of the flow reactor has led us to consider its industrial viability through a cost-benefit analysis, benchmarked against the most advanced existing electrochemical methods. To this end, an extensive techno-economic analysis (TEA) was conducted, factoring in both CO_2-based systems and our system. The electrochemical data for the CO_2-based system using Cu nanopowder as a catalyst is presented in **Supplementary Fig. 30**. Due to the difficulty in detecting C-S species signals, possibly resulting from low FE, we opted to use data from reference 21 for additional TEA calculations. The CO_2 reduction-based system indicates a baseline cost exceeding $2500 per ton for C-S species production at current densities ranging from 20 to 100 mA cm^{-2}, nearly 5 times the cost of our system, as shown in **Fig. 4f**. In addition, we acknowledge the limitations of using the initial proof-of-concept work (ref 21) for comparison, as it may not fully capture the potential of CO_2 reduction technologies,

which continue to advance. Here, we have presented TEA results based on optimized conditions with various parameters for C-S bond formation in the CO_2-reduction system (**Supplementary Fig. 31**). Our system demonstrates a comparable production cost to CO_2-reduction systems with optimized cell voltage and faradaic efficiency (FE = 80%, cell voltage = 3.0 V, current density = 0.1 A). Furthermore, we have provided the levelized cost of HMS and SA production as a function of faradaic efficiency and current density at different cell voltages to offer forward-looking insights into performance targets for future development (**Supplementary Fig. 32 and Supplementary Fig. 33**). To reduce the production cost below $500 per ton of C-S species, the cell voltage should be decreased to below 2.5 V, or alternatively, the FE should be improved to over 80% at higher current densities (>200 mA cm^{-2}). Additionally, current stability remains a challenge for industrial production, and developing high-stability catalysts with enhanced selectivity and activity will be a key focus moving forward.

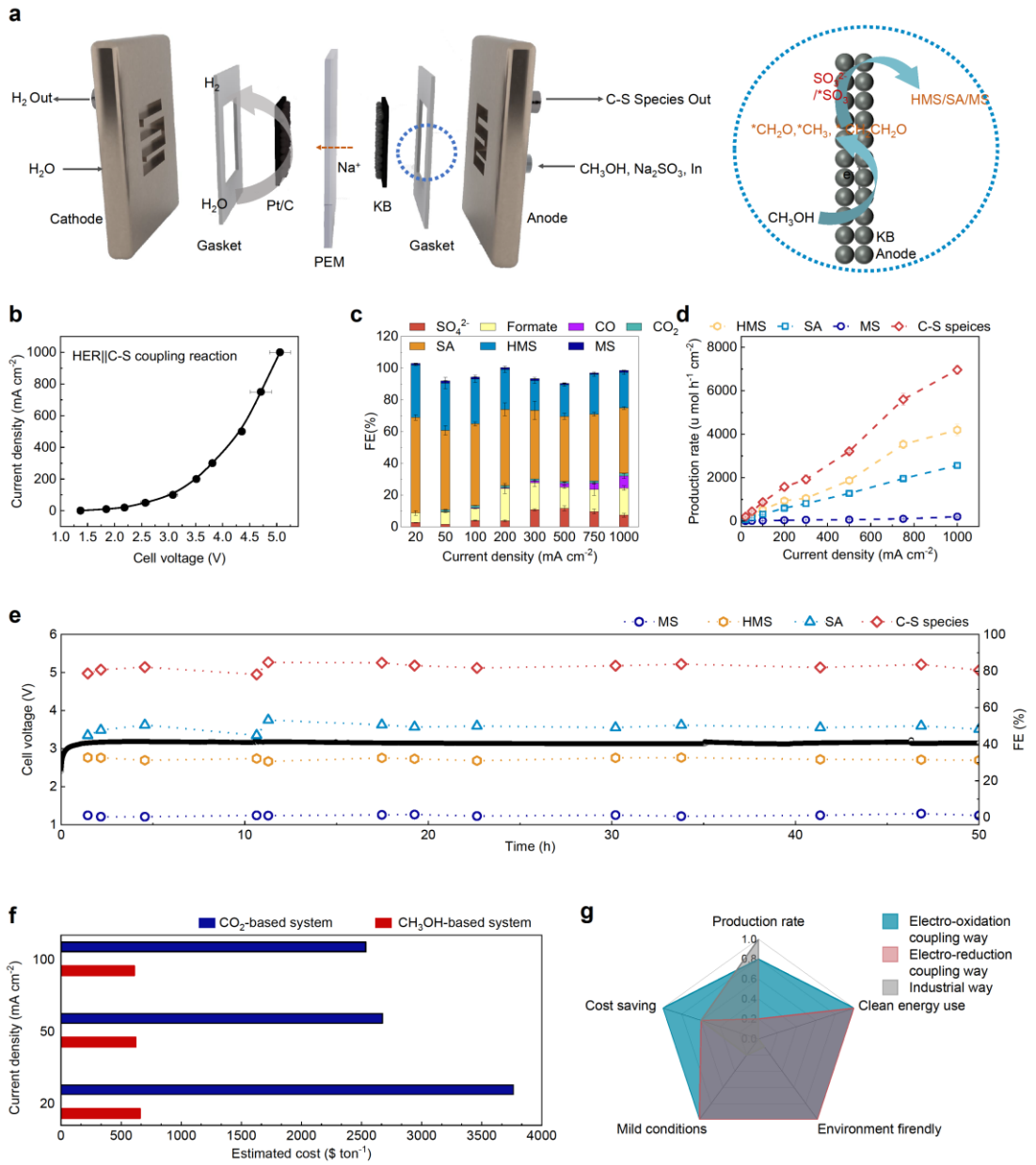

Fig. 4 | Continues electrocatalytic production of C-S species practically. (a) Schematic illustration of a cell configuration for C-S species production. **(b)** The I-V curve of the C-S species production in the flow cell. **(c)** FE of different products obtained at different current densities by using the flow cell. **(d)** production rate of C-S species obtained at different current densities by using the flow cell. **(e)** Chronopotentiometry experiment profile and FE at a current density of 100 mA cm^{-2} for long-term stability. **(f)** Production cost comparison between the electrochemical CO_2 reduction-based and CH_3OH oxidation-based ways. **(g)** A radar plot comparison of different C-S bond constructing technologies. The error bars represent at least three independent tests.

General approach for electrochemical production of diverse C-R species

Our electrochemical approach provides a new route for effectively creating C-S bonds and producing C-S organic molecules at a high production rate. Specifically, the use of commercially available catalysts and the cost-effective feedstocks derived from biomass and industrial waste motivate us to expand this technology for the synthesis of various other C-X materials. Therefore, using a similar design, we explore the possibility of using a diverse range of biomass-derived chemicals as alternative feedstocks.

Employing biomass-derived ethanol, acetate, isopropanol, glycolic acid, glycerol, and ethylene glycol as the activated electrophilic intermediates generation sources, various organosulfurs including the HMS, SA, MS, isethionate (SI) and 1,2-ethane disulfonate (EDS) have been obtained with a considerable high production rate and FE (**Figs. 5a-g** and Supplementary **Figs 34-36**). It is noteworthy that all catalysts employed were commercially available and were directly used without further treatment before using. For example, the SI, which is wildly used in the production of soaps and shampoos,[49] was synthesized through a Pt-catalyzed ethanol coupling reaction, achieving a production rate of 108.99 μmol cm^{-2} hr^{-1}. The EDS, which has been explored as a linker in the synthesis of MOFs,[50] can be generated with the system based on acetate, reaching a production rate of over 800 μmol cm^{-2} hr^{-1}. In addition, for the HMS production, we observed a sixefold increase in production rate in the glycerin-oxidation system compared to the methanol-oxidation system (**Fig. 5i**), indicating strong potential for industrialization. Switching SO_3^{2-} to $S_2O_6^{2-}$ also resulted in the production of similar compounds (**Supplementary Fig 37**). Moreover, this approach proved effective for constructing C-R bonds; using NH_3 as a feedstock led to the formation of formamide, which is traditionally produced from CO and NH_3 under high-temperature and high-pressure conditions (**Supplementary Figs 38 and 39**).[51] In experiments that utilized glycerol as a carbon source, as shown in Fig. 5h, a high production rate of formamide, 300.52 μmol cm^{-2} hr^{-1}, was also achieved.

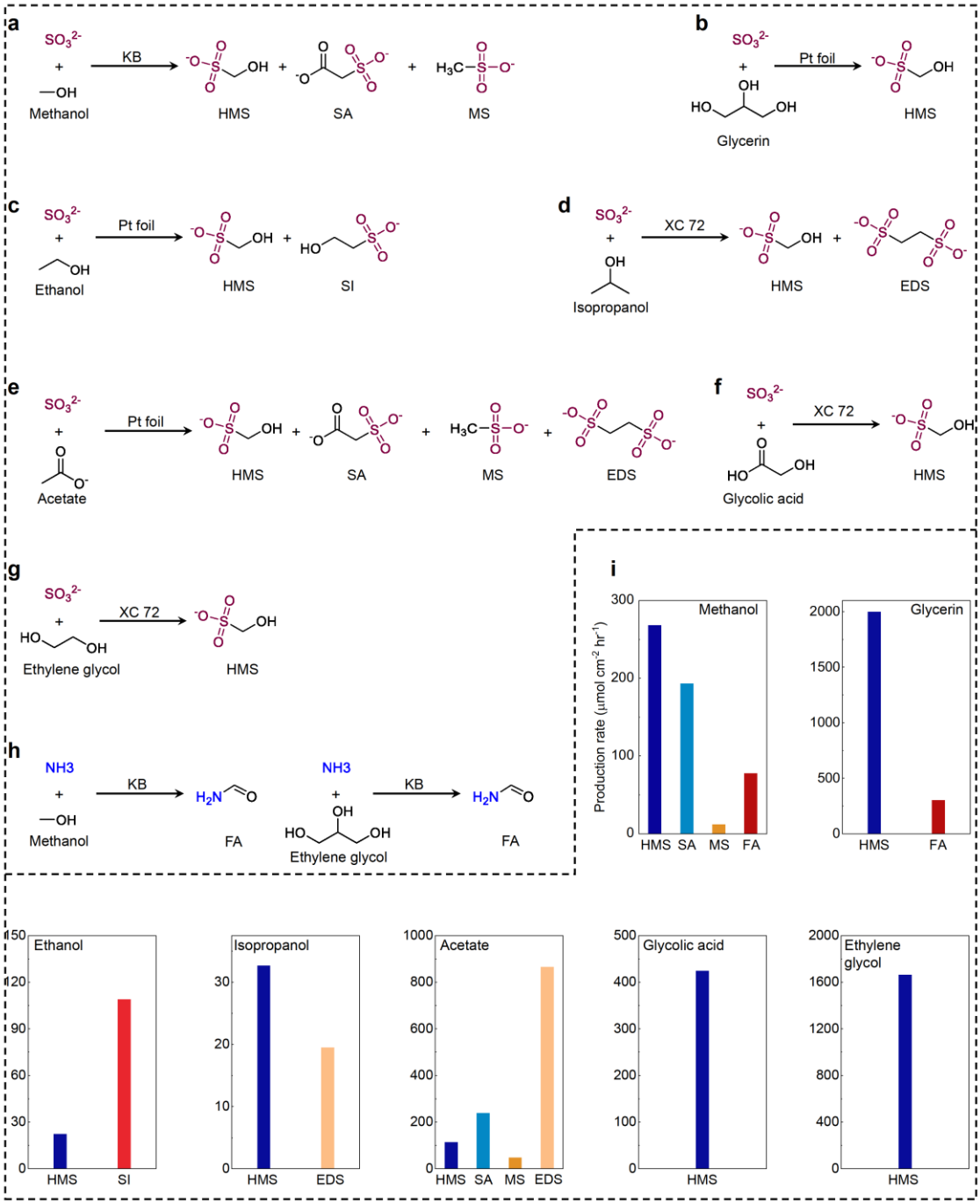

Fig. 5 | General approach for electrochemical C–R bond construction, R is the atom of S, and N. Schematic representation of using various feedstocks for C–R bond formation, employing **(a)** methanol, **(b)** glycerol, **(c)** ethanol, **(d)** isopropanol, **(e)** acetate, **(f)** glycolic acid, and **(g)** ethylene glycol as C sources, and **(h)** ammonia as the N source. **(i)** The production rate of C-R bond formation at 100 mA cm^{-2} by using different electrolytes.

Conclusion

We have developed an efficient and environmentally friendly strategy for constructing C-S bonds through electrochemical upgrading of biomass derivatives using commercial catalysts. Using CH_3OH as the feedstock, we achieve a high efficiency for C-S bond formation, nearly reaching 100% below 10 mA cm^{-2} and exceeding 60% over a wide current density range from 100 to 1000 mA cm^{-2}. An industry-available production rate has been achieved, with 871.67 μmol cm^{-2} hr^{-1} at 100 mA cm^{-2} and 6959.76 μmol cm^{-2} hr^{-1} at 1000 mA cm^{-2}, respectively. Furthermore, our system exhibits excellent long-term durability, showing stability for over 50 hours at a commercial current density of 100 mA cm^{-2} in a practical flow reactor. Different pathways for HMS, SA, and MS formation were identified, and the intermediate including $*CH_2O$, $*CH_3$, and $*OHCH_2CHO$ were proved to be effective in C-S bond formation. Remarkably, our approach demonstrated its flexibility and versatility in creating different C-S bonds from a variety of feedstocks (such as ethanol, acetate, isopropanol, glycolic acid, glycerol, and ethylene glycol) and in forming other types of bonds, such as C-N bonds, making it a promising method for industrial applications in the production of diverse carbon-based compounds.

Data availability

The data that support the plots within this paper and other findings of this study are available from the corresponding authors at reasonable request.

Acknowledgments

X. Z. acknowledges the support from the Hong Kong Polytechnic University (CD9B, WZ4Q, CDBZ), the National Natural Science Foundation of China (22205187), Shenzhen Municipal Science and Technology Innovation Commission (JCYJ20230807140402006), and Department of Science and Technology of Guangdong Province (2023A1515110123, 2024A1515012390).

References

1 Shen, C. H. *et al.* Recent advances in C–S bond formation via C–H bond functionalization and decarboxylation. *Chem. Soc. Rev.* **44**, 291-314 (2015).
2 Dong, B., Shen, J. & Xie, L. G. Recent developments on 1, 2-difunctionalization and hydrofunctionalization of unactivated alkenes and alkynes involving CS bond formation. *Org. Chem. Front.* **10**, 1322-1345 (2023).
3 Xie, P. Z. *et al.* Water-promoted CS bond formation reactions. *Nat. Commun.* **9**, 1321 (2018).
4 Reck, F. *et al.* Identification of 4-substituted 1, 2, 3-triazoles as novel oxazolidinone antibacterial agents with reduced activity against monoamine oxidase A. *J. Med. Chem.* **48**, 499-506 (2005).
5 Organosulfur Compounds Market - Size, Share, Outlook, and Opportunity Analysis, 2022-2028. (2024).
6 Priya, N. Methane Sulfonic Acid Market Research Report Information By Industrial Grade (Industrial, Pharmaceuticals), By Application (Esterification, Electroplating, Pharmaceuticals), And By Region (North America, Europe, Asia-Pacific, And Rest Of The World) –Market Forecast Till 2032 (2024).
7 Natarajan, A. *et al.* Novel arylsulfoanilide− oxindole hybrid as an anticancer agent that inhibits translation initiation. *J. Med. Chem.* **47**, 4979-4982 (2004).
8 Cole, D. C. *et al.* Discovery of 5-arylsulfonamido-3-(pyrrolidin-2-ylmethyl)-1 H-indole derivatives as potent, selective 5-HT6 receptor agonists and antagonists. *J. Med. Chem.* **48**, 353-356 (2005).
9 Barbarella, G., Melucci, M. & Sotgiu, G. The versatile thiophene: an overview of recent research on thiophene-based materials. *Adv. Mater.* **17**, 1581-1593 (2005).
10 Yan, D. *et al.* Synthesis and performance study of sulfur-containing amino acid ammonium phosphate type flame retardants for cotton fabric. *Mater. Today Commun.* **37**, 107180 (2023).
11 Devendar, P. & Yang, G. F. in *Sulfur Chemistry* (ed Xuefeng Jiang) 35-78 (Springer International Publishing, 2019).
12 Xu, Z. B. *et al.* Converting organosulfur compounds to inorganic polysulfides against resistant bacterial infections. *Nat. Commun.* **9**, 3713 (2018).
13 Wang, X. F. *et al.* Organocatalytic Asymmetric Sulfa-Michael/Michael Addition Reactions: A Strategy for the Synthesis of Highly Substituted Chromans with a Quaternary Stereocenter. *Angew. Chem. Int. Ed.* **122**, 8557-8561 (2010).
14 Cong, Z. S. *et al.* N-Heterocyclic carbene-catalyzed sulfa-Michael addition of enals. *Chem. Commun.* **53**, 13129-13132 (2017).
15 Martin, J. G. & Hill, R. K. Stereochemistry of the Diels-Alder Reaction. *Chem. Rev.* **61**, 537-562 (1961).
16 Nicolaou, K. C., Snyder, S. A., Montagnon, T. & Vassilikogiannakis, G. The Diels–Alder reaction in total synthesis. *Angew. Chem. Int. Ed.* **41**, 1668-1698 (2002).
17 Lei, X., Zheng, L., Zhang, C. X., Shi, X. D. & Chen, Y. F. Allylic C–S Bond Construction through Metal-Free Direct Nitroalkene Sulfonation. *J. Org. Chem.* **83**, 1772-1778 (2018).

18 Zhang, X. H., Xu, S., Yang, X. & Pang, W. KI-Catalyzed Allylic Sulfonation of α-Methylstyrene Derivatives with Sulfonylhydrazides via Electrochemistry. *J. Org. Chem.* (2023).
19 Zhang, S. Y. *et al.* Remarkable gas separation performance of a thermally rearranged membrane derived from an alkynyl self-crosslinkable precursor. *J. Membr. Sci.* **672**, 121464 (2023).
20 Singh, M. R. *et al.* Co-pyrolysis of biomass and tires using commercial zeolite and biochar-based catalyst. *Chem. Eng. Process* **187**, 109356 (2023).
21 Li, J. N., Al-Mahayni, H., Chartrand, D., Seifitokaldani, A. & Kornienko, N. Electrochemical formation of C–S bonds from CO_2 and small-molecule sulfur species. *Nat. Synth.* **2**, 757-765 (2023).
22 Kang, H. X. *et al.* Mining the Carbon Intermediates in Plastic Waste Upcycling for Constructing C–S Bond. *J. Am. Chem. Soc.* **146**, 18639-18649 (2024).
23 Huber, G. W., Iborra, S. & Corma, A. Synthesis of transportation fuels from biomass: chemistry, catalysts, and engineering. *Chem. Rev.* **106**, 4044-4098 (2006).
24 Olah, G. A., Goeppert, A. & Prakash, G. S. *Beyond oil and gas: the methanol economy*. (John Wiley & Sons, 2018).
25 Sansaniwal, S., Pal, K., Rosen, M. & Tyagi, S. Recent advances in the development of biomass gasification technology: A comprehensive review. *Renew. Sust. Energ. Rev.* **72**, 363-384 (2017).
26 Xia, Q. *et al.* Methanol-Facilitated Surface Reconstruction Catalysts for Near 200% Faradaic Efficiency in a Coupled System. *Adv. Funct. Mater.*, 2314596 (2024).
27 Zuo, Y. G. & Chen, H. Simultaneous determination of sulfite, sulfate, and hydroxymethanesulfonate in atmospheric waters by ion-pair HPLC technique. *Talanta* **59**, 875-881 (2003).
28 Makarov, S. V. Recent trends in the chemistry of sulfur-containing reducing agents. *Russ. Chem. Rev.* **70**, 885-895 (2001).
29 Rosatzin, T., Bakker, E., Suzuki, K. & Simon, W. Lipophilic and immobilized anionic additives in solvent polymeric membranes of cation-selective chemical sensors. *Anal. Chim. Acta* **280**, 197-208 (1993).
30 Riche, M., Pfeiffer, T. J. & Garcia, J. Evaluation of a sodium hydroxymethanesulfonate product for reducing total ammonia nitrogen in a small-scale rotifer batch culture system. *N. Am. J. Aquac.* **68**, 199-205 (2006).
31 Whiteaker, J. R. & Prather, K. A. Hydroxymethanesulfonate as a tracer for fog processing of individual aerosol particles. *Atmospheric Environ.* **37**, 1033-1043 (2003).
32 Neese, F. The ORCA program system. *Wiley Interdiscip. Rev. Comput. Mol. Sci.* **2**, 73-78 (2012).
33 Lu, T. & Chen, F. W. Multiwfn: A multifunctional wavefunction analyzer. *J. Comput. Chem.* **33**, 580-592 (2012).
34 Yang, R., Li, W. & Chen, N. Reversible chemisorption of nitric oxide in the presence of oxygen on titania and titania modified with surface sulfate. *Appl*

Catal A-Gen. **169**, 215-225 (1998).

35 Watson, J. M. & Ozkan, U. S. Spectroscopic characterization of surface species in deactivation of sol–gel Gd–Pd catalysts in NO reduction with CH_4 in the presence of SO_2. *J. Catal.* **217**, 1-11 (2003).

36 Baral, G. & Marahatta, A. B. FTIR and XRD Characterization of the Cements Available in Commercial Market of Nepal. *Asian J. Appl. Chem. Res.* **14**, 34-53 (2023).

37 Sandt, C. *et al.* Performance comparison of aperture-less and confocal infrared microscopes. *Journal of Spectral Imaging* (2019).

38 Jin, R. B. *et al.* The role of cerium in the improved SO_2 tolerance for NO reduction with NH3 over Mn-Ce/TiO_2 catalyst at low temperature. *Appl. Catal. B* **148**, 582-588 (2014).

39 Wei, L., Cui, S. P., Guo, H. X., Ma, X. Y. & Zhang, L. J. DRIFT and DFT study of cerium addition on SO_2 of manganese-based catalysts for low temperature SCR. *J. Mol. Catal. A: Chem.* **421**, 102-108 (2016).

40 Zhang, C. C. *et al.* Shifting CO_2 hydrogenation from producing CO to CH_3OH by engineering defect structures of Cu/ZrO_2 and Cu/ZnO catalysts. *Chem. Eng. J.* **475**, 146102 (2023).

41 Samant, P. & Fernandes, J. Insitu FTIR studies for the enhanced activity of Pt (HY) and Pt-Ru (HY) zeolite catalysts for electrooxidation of methanol in fuel cells. *Chem. Phys. Lett.* **745**, 137277 (2020).

42 Qi, Y. B. *et al.* Insights into the activity of nickel boride/nickel heterostructures for efficient methanol electrooxidation. *Nat. Commun.* **13**, 4602 (2022).

43 Chen, X. *et al.* Highly Stable Layered Coordination Polymer Electrocatalyst toward Efficient CO_2-to-CH_4 Conversion. *Adv. Mater.* **36**, 2310273 (2024).

44 Lima, M. *et al.* CO_2 reduction on Cu/C used as a cathode in a polymeric electrolyte reactor-Fuel cell type. *Int. J. Hydrog. Energy* **47**, 4010-4017 (2022).

45 Barbosa, A. F., Del Colle, V., Galiote, N. A. & Tremiliosi-Filho, G. Effect of tin deposition over electrogenerated random defects on Pt (111) surfaces onto ethanol electrooxidation: Electrochemical and FTIR studies. *J. Electroanal. Chem.* **857**, 113734 (2020).

46 Chen, Y. X. *et al.* Application of in-situ attenuated total reflection-fourier transform infrared spectroscopy for the understanding of complex reaction mechanism and kinetics: formic acid oxidation on a Pt film electrode at elevated temperatures. *J. Phys. Chem. B* **110**, 9534-9544 (2006).

47 Bagchi, D. *et al.* Structure-Tailored Surface Oxide on Cu–Ga Intermetallics Enhances CO_2 Reduction Selectivity to Methanol at Ultralow Potential. *Adv. Mater.* **34**, 2109426 (2022).

48 Lin, Y. *et al.* Inspiration of Bimetallic Peroxide for Controllable Electrooxidizing Ethylene Glycol Through Modulating Surficial Intermediates. *Adv. Funct. Mater*, 2404594 (2024).

49 Umbach, W. *Kosmetik und Hygiene: von Kopf bis Fuß*. (John Wiley & Sons, 2012).

50 Sun, M. X. *et al.* Preparation of ionic covalent organic frameworks and their

applications in solid-phase extraction. *Trends Analyt. Chem.* **157**, 116829 (2022).
51 Shindell, D. & Smith, C. J. Climate and air-quality benefits of a realistic phase-out of fossil fuels. *Nature* **573**, 408-411 (2019).